

We are IntechOpen, the world's leading publisher of Open Access books Built by scientists, for scientists

4,800

Open access books available

122,000

International authors and editors

135M

Downloads

Our authors are among the

154

Countries delivered to

TOP 1%

most cited scientists

12.2%

Contributors from top 500 universities

**WEB OF SCIENCE™**Selection of our books indexed in the Book Citation Index
in Web of Science™ Core Collection (BKCI)

Interested in publishing with us?
Contact book.department@intechopen.com

Numbers displayed above are based on latest data collected.

For more information visit www.intechopen.com

Image Processing for Optical Metrology

Miguel Mora-González, Jesús Muñoz-Maciel, Francisco J. Casillas,
Francisco G. Peña-Lecona, Roger Chiu-Zarate
and Héctor Pérez Ladrón de Guevara
*Universidad de Guadalajara, Centro Universitario de los Lagos
México*

1. Introduction

Optical measurements offer the desirable characteristics of being noninvasive and nondestructive techniques that are able to analyze in real time objects and phenomena in a remote sense. Science areas that involve optical characterization include physics, biology, chemistry and varied fields of engineering. The use of digital cameras to record objects or a specific phenomenon permits the exploitation of the potential of that the associated images can be processed to determine one or several parameter or characteristics of what is being recorded. These images need to be processed and securely there will be a model associated with the optical metrology that will provide an insight or a comprehensive understanding of the image being analyzed. Matlab® is the suitable platform to implement image processing algorithms due to its ability to perform the whole processing techniques and procedures to analyze and image. At the same time it provides a flexible and a fast programming language for user constructing algorithms. In the present chapter we provide some fundamentals about image acquisition, filtering and processing, and some applications. Some applications are well-know techniques while others offer the state of the art in the field under study. All authors agree that Matlab® is a powerful tool for image processing and optical metrology.

All algorithms and/or sentences used in this chapter are made in such manner so that they work in the Matlab® R2007b platform or superior. Matlab® is a trade mark of Mathworks Inc., from here on we will refer it as Matlab only. Also the Matlab functions and parameters used along the chapter are typed in italics and in apostrophes, respectively.

Algorithms in present chapter are presented in two formats depending on the algorithm extension: 1) Image titles and/or figure captions for low algorithms extension; 2) Subsection ends for larger algorithms.

2. Image processing and acquisition

In the present section, image and processing acquisition principles in Matlab are established.

2.1 Image acquisition

Image acquisition is the initial stage in every vision system for human or artificial image data interpretation. Image acquisition is the recording process of a real object, this implies

that the vision process totally depends on quality acquisition; this could be an analogical or digital. The analogical acquisition process is a representation of the object with several techniques like designing, painting, photography, and video. In a similar way, digital imaging acquisition is able to represent a real object, however object properties are presented in a discrete form. Every object characteristics are mapped from a real plane to a digital plane where a group of discrete values (i.e 1, 2, 3, ...) represent position, form, color and texture.

2.1.1 Acquisition and digital image representation

Image acquisition process in Matlab can be done by the use of either *imread* or *getsnapshot* functions for stored images or video, respectively. Each function stores the object representation in a discrete $l \times m \times n$ array, where l can be related to color data; m and n indexes represent the image spatial coordinates.

An example of a real image is shown in Figure 1a, and in Figure 1b, the representation in a matrix array of the selected area from the image. Digital images are described as a bi-dimensional $f(x,y)$ function, where x and y represent the spatial coordinates. The f value at the (x,y) position point is proportional to the intensity or gray scale of the image.

In Matlab, a digital image satisfies following conditions: first, spatial and gray scale values must be discrete; and second, intensities are sampling at 8 bits (255 values).

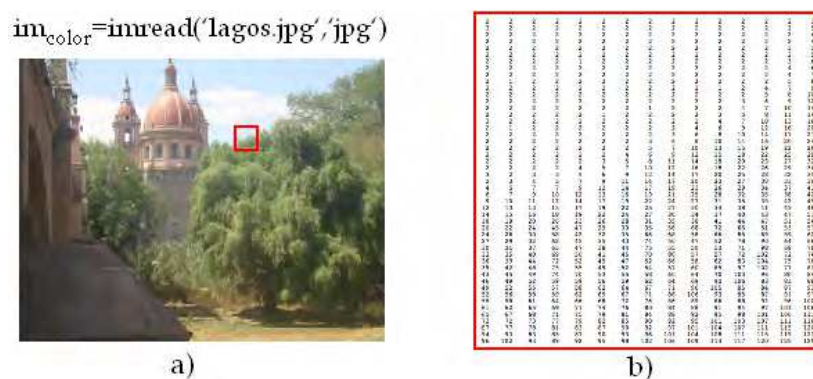


Fig. 1. a) real color image, and b) matrix of the green color component of the selected area.

2.1.2 Image discretization

Image discretization is the process of converting an analogical image to a digital image; this process depends on the sampling and quantization stages.

Correspondence between analogical and digital images is given by the number of pixels used. If the number of pixels is enough to satisfy the Nyquist criteria (Oppenheim et al., 1997), the acquired image is a satisfactory representation of the real object observed. Quantization is the process of assigning a color or gray discrete level to each sample.

Therefore, image discretization quality depends on frequency sampling as in quantization levels used. It must be noted that Matlab only reads digital images. Acquisition process can be done with scanners, CCD cameras, etc.

2.2 Thresholding and high contrast image

Frequently, acquired images under real conditions present a background problem. When relevant foreground elements are mixed with low interest background ones. Another

problem that hides the desired information is a low contrast image. Therefore, the use of algorithms that deals with can be implemented in order to enhance the images. Equalization, binarization and thresholding algorithm are alternatives that have proved to be successful.

In the following subsection, a method for the conversion of color images into gray levels is presented. Next, by using histogram equalization, a high contrast image from the gray scale levels is obtained. Finally, binarization process by establishing a thresholding is described in order to get a two color image (black (0) and white (255)) from a gray level scale (Poon & Banerjee, 2001).

2.2.1 Histogram

Histogram is the graphical representation of pixels gray values distribution. Images can be classified according to its histogram as high, medium or low contrast images. A low contrast image has a histogram with a low fraction of all possible gray values, around less than 40% of the whole scale. A high contrast image has more than 90% of the gray values.

Color images can also be classified in accordance with its histogram by considering human ocular sensitivity to primary colors. This is given by the first component of the YIQ matrix:

$$Y = 0.299R + 0.587G + 0.114B, \quad (1)$$

Where Y and RGB are the lumma components used in color television systems NTSC (that represents a gray scale in the YIQ space) and the primary components, red, green and blue, respectively. The histogram transformation for a color image is given by the following pixel to pixel operation:

$$T_{gsl}(r_k) = s_k, \quad (2)$$

where r_k and s_k are the original pixel intensities in color and gray scale levels (gsl) respectively. In figure 2 is shown the image obtained by the use of equation (2) and its corresponding histogram, these operations can be done by using the Matlab functions `rgb2gray` and `imhist`.

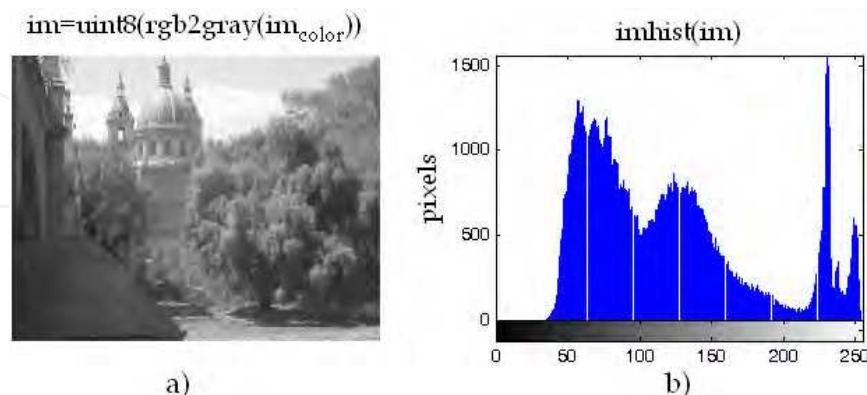


Fig. 2. a) gsl photography, b) histogram.

2.2.2 Histogram equalization

Histogram equalization is the transformation of the intensity values of an image that is typically applied to enhance the contrast of the image. As an example, the contrast of the

image of the figure 2a, can be handled by applying histogram equalization and it is shown in figure 3 with its respective histogram, this operation can be done by using the Matlab function *histeq*.

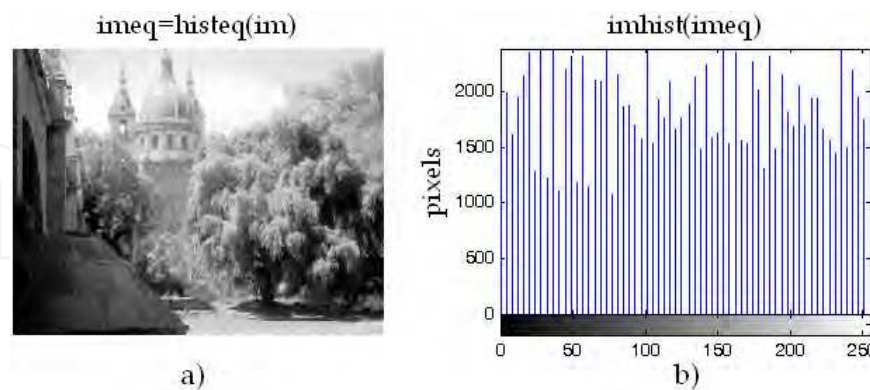


Fig. 3. a) Photography equalization, b) histogram.

In order to get the discrete values in a gsl, the following equation is used

$$T_{eq}(s_k) = \sum_{j=0}^k \frac{n_j}{n} (L-1), \quad (3)$$

where $k = 0, 1, 2, \dots, (L-1)$, L represents the gray level numbers into an image (255 as an example), n_j is the frequency of appearance of an specific j -th gray level and n is the total number of pixels of the image.

2.2.3 Thresholding by histogram

Thresholding is a non-linear operation for image segmentation that consists in the conversion of a gsl image into a binary image according to a threshold value. This operation is used to separate some regions of the foreground of an image from its background. Thresholding operation can be done by using the Matlab function *graythresh*. Binarization may be considered as an especial case of thresholding as shown in figure 4. The Matlab function that binaries an image is *im2bw*.



Fig. 4. Image binarization by thresholding.

2.3 Spatial filtering

In order to reduce noise or enhance some specific characteristics of an image some filters like high-pass, low-pass, band-pass or band-stop are used. These filters can be applied in the

frequency domain (section 2.4) or in the spatial domain. Spatial domain filtering is described in this section. Filtering operations are directly applied to the image (pixel to pixel). The mathematical functions applied in the spatial domain are well known as convolution, and are described by (Mora-González et al., 2008)

$$f(x,y) * g(x,y) = \sum_{m=-\frac{M+1}{2}}^{\frac{M+1}{2}} \sum_{n=-\frac{N+1}{2}}^{\frac{N+1}{2}} f(m,n)g(x-m,y-n), \quad (4)$$

where $f, g(x,y), (m,n)$ and $M \times N$ are the original image, the convolution mask or matrix, the original image coordinates, the coordinates where the convolution is performed, and the size of convolution mask, respectively. Equation (4) is applied by doing a homogeneous scanning with the convolution mask versus the whole image to be convolved. These filters are also known as Finite Impulse Response (FIR) filters because they are applied to a finite section of the spatial domain (In this case the finite section is the image). Equation (4) can be implemented in Matlab by using nested *for* loops, also *conv2*, *fspecial* or *imfilter* functions can be used too. These kinds of filters are dependent of the convolution mask form as is explained in the following two subsections.

2.3.1 Low-pass filters

Low-pass filters applied to images have the purpose of image smoothing, by blurring the edges into the image and lowering the contrast. The main characteristic of a low-pass convolution mask is that all of its elements have positive values. Some commonly used low-pass filters are: averaging, gaussian, quadratic, triangular and trigonometric. These mask are presented in a matrix form like

$$g(m,n) = \frac{1}{\sum_{m=1}^M \sum_{n=1}^N w_{m,n}} \begin{bmatrix} w_{1,1} & w_{1,2} & \dots & w_{1,N} \\ w_{2,1} & w_{2,2} & \dots & w_{2,N} \\ \vdots & \vdots & \ddots & \vdots \\ w_{M,1} & w_{M,2} & \dots & w_{M,N} \end{bmatrix}, \quad (5)$$

with

$$w = \left\{ \begin{array}{l} A \exp\left(-B\left[\left(m - \frac{M+1}{2}\right)^2 + \left(n - \frac{N+1}{2}\right)^2\right]\right), \quad \text{gaussian} \\ A\left[1 - B\left(m - \frac{M+1}{2}\right)^2 - B\left(n - \frac{N+1}{2}\right)^2\right], \quad \text{cuadratic} \\ \frac{A}{2} + \frac{A}{4} \cos\left[B\left(m - \frac{M+1}{2}\right)\right] + \frac{A}{4} \cos\left[B\left(n - \frac{N+1}{2}\right)\right], \quad \text{trigonometric} \\ A, \quad \text{average} \end{array} \right\}, \quad (6)$$

where A, B and w are the amplitude, the width function factor and the weight function of the spatial filter, respectively. In order to determine the effectiveness of the masks of the equations (5) and (6), Magnitude Spectra (MS) are obtained to analyze the low frequencies allowed to pass by the filter and high frequencies attenuation. This is expressed as

$$MS(\omega) = 20 \log |\mathfrak{F}\{g(m,n)\}|, \quad (7)$$

where ω and \mathcal{F} are the MS frequency component and the Fourier transform operator, respectively.

In figure 5, the MS of the convolution mask from equations (5) and (6) are shown. Spatial gaussian filter behavior is more stable because allows low frequencies to pass and also attenuate middle and high frequencies faster than other filters, as can be observed. The mask for nine elements is shown in table 1. It must be mentioned that the processing time slow down conforming the convolution mask increases. Spatial filtering also has a problem in the image edges, because they cannot be convolved and there are $(M-1)/2$ and $(N-1)/2$ lost information elements in x and y axes, respectively. By using the *fspecial* function, low-pass masks can be generated by applying the 'gaussian' or 'average' Matlab parameters.

Another mask types designed for signal processing can be implemented on image processing by a two dimensional extension. In figure 6 it is shown three different low-pass filters applied in the test image.

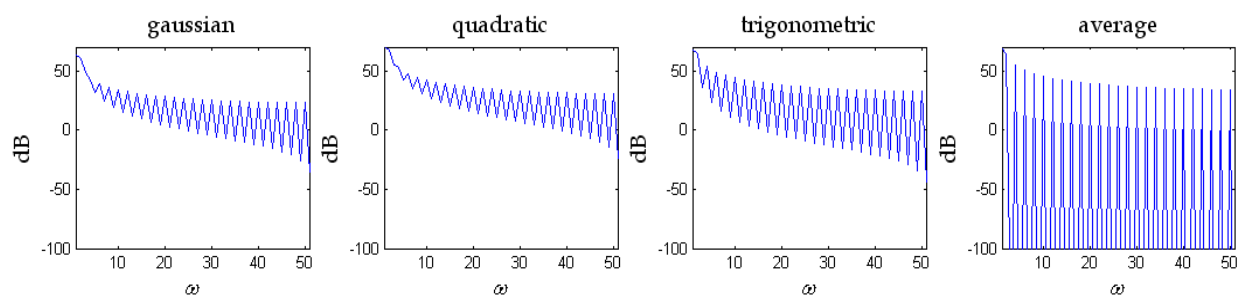


Fig. 5. MS of equations (5) and (6) masks, with $A=1$, $B=1$ and $w=1$. Matlab code representation of equation (7) is: $MS=20*\log_{10}(abs(fft(g)))$.

Gaussian	Quadratic	Trigonometric	Average
$\begin{pmatrix} .0449 & .1221 & .0449 \\ .1221 & .3319 & .1221 \\ .0449 & .1221 & .0449 \end{pmatrix}$	$\begin{pmatrix} 0 & .1667 & 0 \\ .1667 & .3333 & .1667 \\ 0 & .1667 & 0 \end{pmatrix}$	$\begin{pmatrix} .1011 & .1161 & .1011 \\ .1161 & .1312 & .1161 \\ .1011 & .1161 & .1011 \end{pmatrix}$	$\frac{1}{9} \begin{pmatrix} 1 & 1 & 1 \\ 1 & 1 & 1 \\ 1 & 1 & 1 \end{pmatrix}$

Table 1. 3x3 convolution masks g for low-pass filters of equations (5) and (6), with $A=1$, $B=1$ and $w=1$.

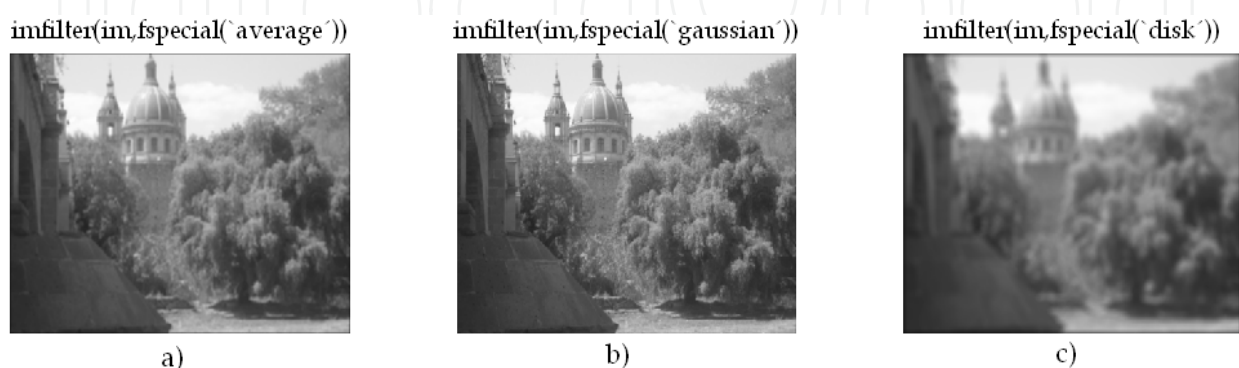


Fig. 6. Low-pass 3x3 filters examples applied to figure 1a. Matlab parameters used: a) average, b) gaussian and c) disk.

2.3.2 High-pass filters

High frequency components are mostly located in image borders, like fast tone changes and marked details. The main purpose of a high-pass filter is to highlight the image details for skeletonizing, geometrical orientation, contrast enhancement, and revealing hidden characteristics, among many others. One of the most common high-pass spatial filters is the high-boost that consists in an interactive subtraction process between the original image and low-pass filters. The weighting function for a 3x3 matrix is obtained by

$$w = \begin{cases} 9C - \frac{1}{9}, & m = 2, n = 2 \\ -\frac{1}{9}, & m \neq 2, n \neq 2 \end{cases} \quad (8)$$

The differential filters are another kind of high-pass filters that get its weighting function based on the partial derivatives applied to the image. The most usual differential filters are the gradient and laplacian, based on the following equations

$$|\nabla(f(x,y))| = \sqrt{\left(\frac{\partial f}{\partial x}\right)^2 + \left(\frac{\partial f}{\partial y}\right)^2} \approx \left|\frac{\partial f}{\partial x}\right| + \left|\frac{\partial f}{\partial y}\right|, \quad \text{gradient magnitude}, \quad (9)$$

and

$$\nabla^2(f(x,y)) = \frac{\partial^2 f}{\partial x^2} + \frac{\partial^2 f}{\partial y^2}, \quad \text{laplacian}, \quad (10)$$

if the magnitude of the partial derivatives work with a 3x3 mask, then

$$\left|\frac{\partial f}{\partial x}\right| = \frac{1}{\kappa + 2} [(w_{1,3} + \kappa \cdot w_{2,3} + w_{3,3}) - (w_{1,1} + \kappa \cdot w_{2,1} + w_{3,1})] \quad (11)$$

and

$$\left|\frac{\partial f}{\partial y}\right| = \frac{1}{\kappa + 2} [(w_{1,1} + \kappa \cdot w_{1,2} + w_{1,3}) - (w_{3,1} + \kappa \cdot w_{3,2} + w_{3,3})]. \quad (12)$$

Other used filters based on gradients are the Sobel, Prewitt and Canny. The Sobel spatial filter uses the central weight constant $k=2$ (Pratt, 2001). Meanwhile the Prewitt space filter uses $k=1$. The Canny space filter uses two different thresholds for weak and strong edges detection (Canny, 1986). Table 2 shows the nine elements masks of the most utilized high-pass filters. Figure 7 shows six examples of the application of these functions as high-pass filters to figure 1a. It is observed that the Canny filter is the most powerful edge detector filter.

2.4 Mathematical discrete transforms

Discrete transform analysis has played an important role in digital image processing. Several transform types are applicable to digital image processing, but due to their optical metrology potential applications, Fourier and Radon transforms are presented in this chapter section.

2.4.1 Fourier transform

Discrete Fourier Transform (DFT) represents the change from spatial to frequency domain. In convergent optical systems this transform represents the propagated optical perturbation from exit pupil to the focal point in a single lens arrangement. Equations (13) and (14) represent the DFT pair for the mathematical two dimensional (2D) model (Gonzalez, 2002)

$$\mathfrak{F}\{f(x,y)\} = F(u,v) = \frac{1}{MN} \sum_{x=1}^M \sum_{y=1}^N f(x,y) \exp\left[-i2\pi\left(\frac{ux}{M} + \frac{vy}{N}\right)\right], \quad (13)$$

Sobel		Prewitt		Gradient		Laplacian
$\left \frac{\partial f}{\partial x}\right =$	$\left \frac{\partial f}{\partial y}\right =$	$\left \frac{\partial f}{\partial x}\right =$	$\left \frac{\partial f}{\partial y}\right =$	$\left \frac{\partial f}{\partial x}\right =$	$\left \frac{\partial f}{\partial y}\right =$	$\begin{pmatrix} 0 & 1 & 0 \\ 1 & -4 & 1 \\ 0 & 1 & 0 \end{pmatrix}$
$\begin{pmatrix} 1 & 0 & -1 \\ 2 & 0 & -2 \\ 1 & 0 & -1 \end{pmatrix}$	$\begin{pmatrix} 1 & 2 & 1 \\ 0 & 0 & 0 \\ -1 & -2 & -1 \end{pmatrix}$	$\begin{pmatrix} 1 & 0 & -1 \\ 1 & 0 & -1 \\ 1 & 0 & -1 \end{pmatrix}$	$\begin{pmatrix} 1 & 1 & 1 \\ 0 & 0 & 0 \\ -1 & -1 & -1 \end{pmatrix}$	$\begin{pmatrix} 1 & 1 & -1 \\ 1 & -2 & -1 \\ 1 & 1 & -1 \end{pmatrix}$	$\begin{pmatrix} 1 & 1 & 1 \\ 1 & -2 & 1 \\ -1 & -1 & -1 \end{pmatrix}$	

Table 2. Some 3x3 convolution masks g for high-pass differential filters (Bow, 2002).

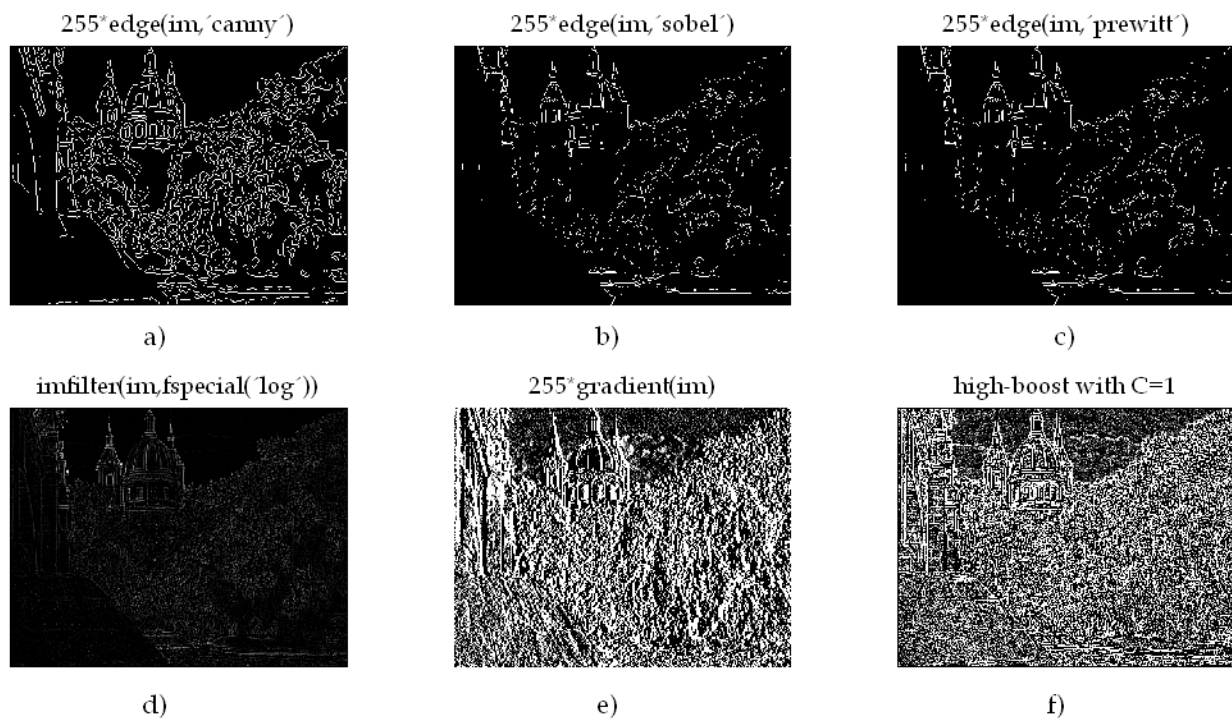


Fig. 7. High-pass 3x3 filters examples applied to figure 1a. Matlab parameters and functions used: a) 'canny', b) 'sobel', c) 'prewitt', d) laplacian with 'log', e) *gradient* and f) high-boost filter.

and

$$\mathfrak{F}^{-1}\{F(u,v)\} = f(x,y) = \sum_{u=1}^M \sum_{v=1}^N F(u,v) \exp\left[i2\pi\left(\frac{ux}{M} + \frac{vy}{N}\right)\right], \quad (14)$$

where (u,v) , $M \times N$ and \mathfrak{F}^{-1} are the Fourier space coordinates, the image size, the inverse Fourier transform operator, respectively. Matlab has *fft2* and *ifft2* special functions for equations (13) and (14), respectively, where FFT is the acronym of Fast Fourier Transform. Other functions of Fourier transforms are *fft*, *ifft* for one dimension, and *fftshift* for the shifting of the zero-frequency component to spectra center. An important characteristic obtained from the Fourier transform is that it gives the frequencies content of the image. Due to this property, frequency filter design is a very straight forward task. Low frequencies are located into the matrix around the central coordinates, while frequencies gradually increase as are spread out from its center in a radial form. This characteristic is ideal for frequency filtering (low-pass, high-pass, band-pass, and band-stop). The frequency filtering process consists in the multiplication between image Fourier transform with a binary circular mask. Figure 8 shows the filtered Fourier spectra and the resulting filtered images for a high-pass, low-pass, band-pass and band-stop.

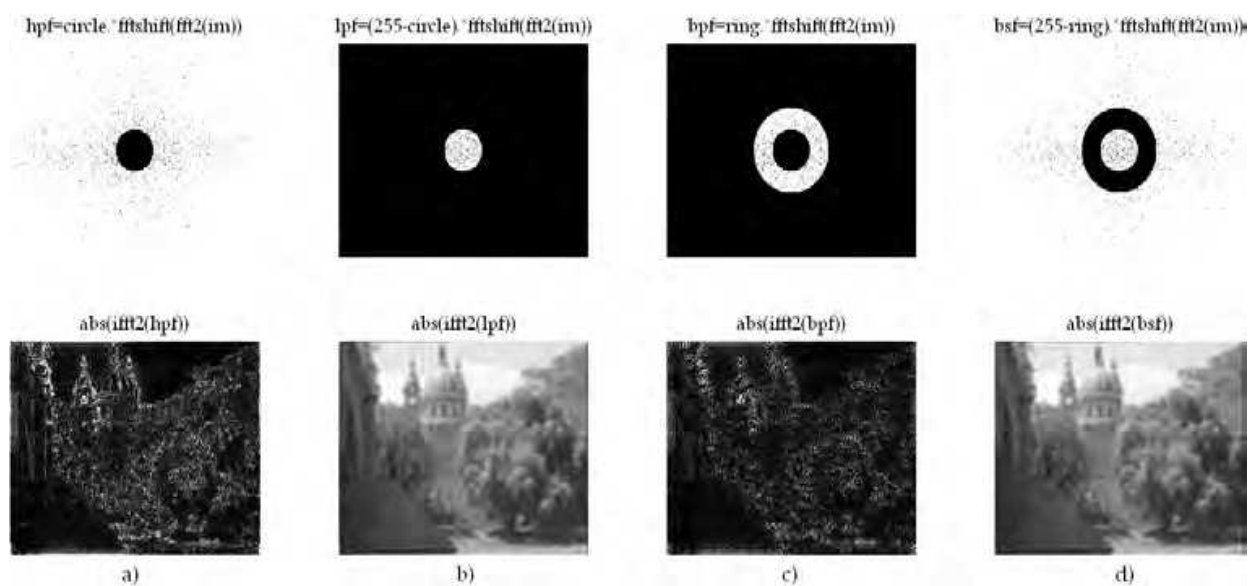


Fig. 8. Fourier filtering applied to figure 1a. a) high-pass, b) low-pass, c) band-pass and d) band-stop. Where, circle and ring are masks of 30 and 60 pixels radii.

2.4.2 Radon transform

Radon transform applied in pattern recognition or digital image processing may be considered as the image's grayscale projection over a given angle with respect to x axis. The mathematical model of the Radon transform is (Bracewell, 1995)

$$\mathfrak{R}\{f(x,y)\} = \int_{-\infty}^{\infty} \int_{-\infty}^{\infty} f(x,y) \delta(R - x \cos \theta - y \sin \theta) dx dy, \quad (15)$$

where \mathfrak{R} , δ , R and θ are the Radon transform operator, the Dirac delta function, the distance from the origin to the profile line and the angle of direction of the same line, respectively. Each of these parameters can be observed in figure 9, Q is the origin of the profile line to be obtained (thick blue bold line). Equation (15) is implemented in Matlab with the special function *radon*.

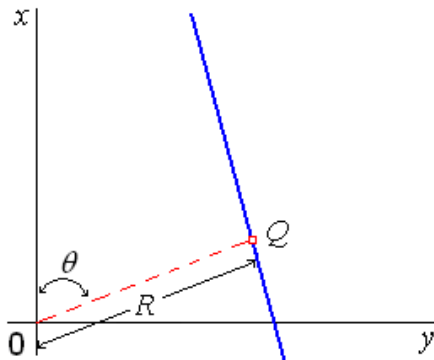


Fig. 9. Radon transform parameters.+

3. Optical metrology fundamentals

Optical metrology is a field of physics that include theoretical and experimental methods to estimate physical parameters using the light wavelength as fundamental scale.

3.1 Optical interferometry

Optical interferometry is based in the light interference phenomenon to determine different physical variables. A typical application is in nondestructive optical testing that requires high accuracy. The interferometer is the optical system used by this technique, which allows by interfering fringes the estimation of deformation components, shapes, strains or vibrations in objects with polished or rough surfaces. According to users' requirements, different configurations of interferometers can be selected to measure displacements components.

3.1.1 Interference

Figure 10 shows the schematic of a common optical arrangement used in interferometry well known as Michelson interferometer. The beam splitter (BS) splits the incident collimated laser light in two wavefronts that propagate in different directions and are reflected by the plane mirrors M1 and M2 respectively, and then they are combined with the same BS to form an interference pattern that can be observed directly on the screen.

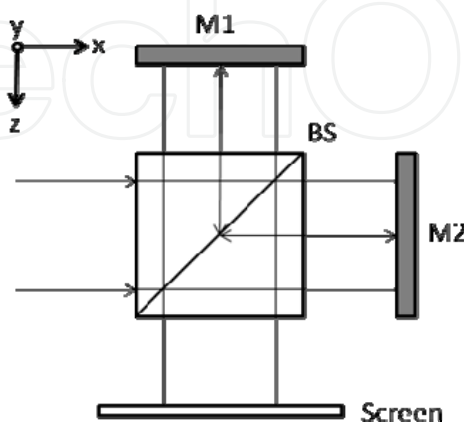


Fig. 10. Michelson interferometer.

The superposition of the two wavefronts at a position (x,y) is expressed by the complex sum:

$$U(x, y) = a_1(x, y) \exp[i\phi_1(x, y)] + a_2(x, y) \exp[i\phi_2(x, y)], \quad (16)$$

where $a_1(x, y)$ and $a_2(x, y)$ are the amplitudes and its respective phases $\phi_1(x, y)$ y $\phi_2(x, y)$. The intensity at a point in the interference pattern is determined with the product of perturbation U multiplied by its complex conjugated U^* , this is

$$I(x, y) = U(x, y) \cdot U^*(x, y), \quad (17)$$

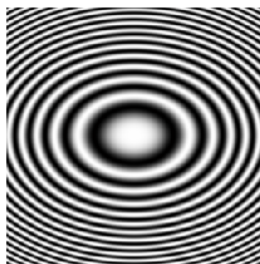
then, the resulting intensity is given by

$$I(x, y) = I_1(x, y) + I_2(x, y) + 2\sqrt{I_1(x, y)I_2(x, y)} \cos[\phi(x, y)], \quad (18)$$

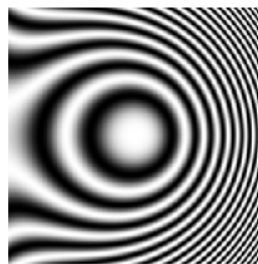
where $I_1(x, y) = a_1^2(x, y)$ and $I_2(x, y) = a_2^2(x, y)$ are the intensities for each wavefront and $\phi(x, y)$ is the phase difference between them, since these propagate along to different paths before the interference.

Due to cosine of equation (18), $I(x, y)$ reaches its maxima when $\phi(x, y)$ corresponds to even multiples of π (constructive interference) and its minima for odd multiples of π (destructive interference) (Gasvik, 2002). In general, optical interferometry is applied to estimate this phase difference, which can arise due to geometrical variations or deformations in a testing object. In figure 11 are shown two synthetic interference patterns when is replaced a mirror: a) with tilt in y and defocus and b) with defocus and coma in the interferometer of figure 10. The phase difference involving the geometrical variations of the mirrors is given by $\phi(x, y) = 4\pi\Delta z/\lambda$, where λ is the wavelength of the illumination source and Δz is the shape phase difference introduced by the mirrors.

$$YD = 5 + 5 \cdot \cos(C_1 \cdot (2 \cdot (y-N)^2 + (x-N)^2)) \quad DC = 5 + 5 \cdot \cos(C_1 \cdot ((y-N)^2 + (x-N)^2) + C_2 \cdot ((y-N)^2 + (x-N)^2) \cdot (x-N))$$



a)



b)

Fig. 11. Fringe patterns of mirrors with: a) tilt in y and defocus, YD; and b) defocus and coma, DC. These wavefronts were generated using nested for loops. For these cases $N=128$ pixels; $C_1=0.01$ and $C_2= 0.00001$ are the numerical parameter of each aberration.

Another way to generate fringe patterns is by replacing a mirror of the interferometer for a testing object with an optically rough surface that experiments a deformation. In this case, the interference fringe pattern is not observed directly on the screen as in the previous described case. The superposition of a wavefront reflected by a rough surface (object beam) with a regular wavefront (reference beam) as the reflected by a plane mirror in the Michelson interferometer causes that I_1 , I_2 and ϕ of equation (18) vary fast and randomly, normally obtaining a speckle pattern. In speckle pattern interferometry the fringe patterns are obtained by the correlation of two speckle patterns recorded using a CCD camera placed at the screen position of the interferometer for the object before and after a deformation $\Delta\phi(x, y)$. Assuming $I_i(x, y)$, $I_f(x, y)$ are the intensities of the speckle patterns for the initial no-

deformed state and the final deformed state respectively, the fringe pattern can be calculated by (Lehmann, 2001)

$$|I_f(x,y) - I_i(x,y)|, \quad (19)$$

and the phase difference involving the deformation of the object is given by $\Delta\phi(x,y) = 4\pi z' / \lambda$, where z' is the displacement of the object in z direction (Waldner, 2000).

3.1.2 Phase shifting

In order to determine the phase $\phi(x,y)$ from fringe patterns, is applied a procedure well-known as phase shifting. For this procedure can be registered several images introducing a phase difference which experimentally is achieved with a piezoelectric (PZ) that modifies the optical path length of one of the beams. A widely used algorithm to calculate the phase employs four consecutive images shifted by $\pi/2$ (Huntley, 2001)

$$\phi(x,y) = \tan^{-1} \left[\frac{I_d(x,y) - I_b(x,y)}{I_a(x,y) - I_c(x,y)} \right], \quad (20)$$

where $I_a(x,y)$, $I_b(x,y)$, $I_c(x,y)$ and $I_d(x,y)$ are the intensities of the shifted images. Due to the inverse tangent, in this pattern arise an effect of wrapping in a 2π module; moreover can be affected by noise of high frequency in the case of speckle interferograms. If the interest of the user is to explore the reduction of speckle noise and phase unwrapping techniques can consults references (Sirohi, 1993) and (Ghiglia, 1998).

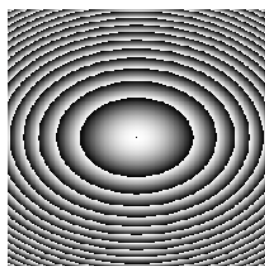
In figure 12 are shown the wrapped phases calculated with equation (20) using the fringe patterns presented in the section.

3.2 Image diffraction

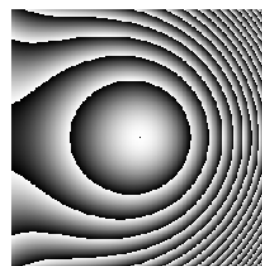
The mathematical representation for a collimated wavefront passing through a convergent optical system until the focal point is given by the Fourier transform, as is observed in figure 13. By setting a diffraction grating in the entrance pupil of a convergent lens, a Fraunhofer diffraction pattern is obtained in the focal point (Goodman, 2005), given by

$$U_o(u,v) = \frac{A \cdot \exp \left[j \frac{\pi}{f\lambda} (u^2 + v^2) \right]}{j\lambda f} \int_{-\infty}^{\infty} \int r(x,y) \cdot \exp \left[-j \frac{2\pi}{f\lambda} (xu + yv) \right] dx dy, \quad (21)$$

$$\text{wpYD} = 255 * (\text{atan2}(\text{YD}_d - \text{YD}_b, \text{YD}_a - \text{YD}_c) + \pi) / (2\pi) \quad \text{wpDC} = 255 * (\text{atan2}(\text{DC}_d - \text{DC}_b, \text{DC}_a - \text{DC}_c) + \pi) / (2\pi)$$



a)



b)

Fig. 12. Calculated wrapped phases for: a) tilt in y and defocus, wpYD; and b) defocus and coma, wpDC.

where $U_0(u, v)$, $r(x, y)$, A and λ are the complex amplitude distribution of the field in the back focal plane of the lens, the grating function, the amplitude of the monochromatic plane wave and the illumination wavelength, respectively. The result of equation (21) varies depending on the function of the grating. For our purposes, those functions are binary and sinusoidal.

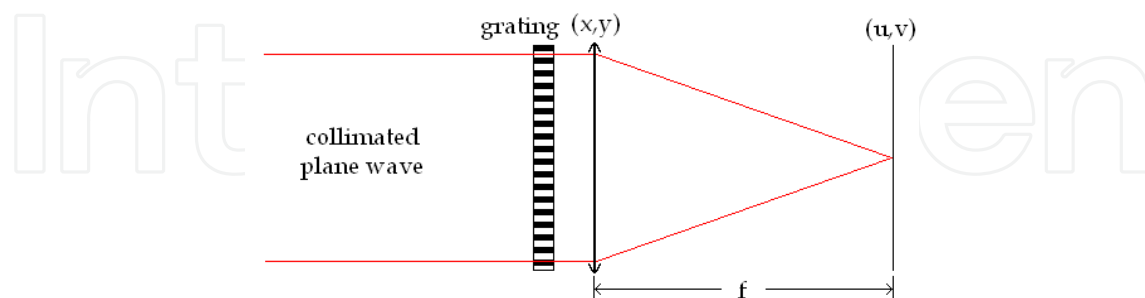


Fig. 13. Diagram for performing the Fourier transform of a grating with a positive lens.

3.2.1 Binary grating

A binary grating can be mathematically represented by a Fourier series expansion of a step function (f_{step}) bounded in the $[0, T]$ interval, see figure 14a. The function is defined by:

$$f_{step}(x, y) = \begin{cases} a, & 0 < y < \frac{T}{2} \\ 0, & \frac{T}{2} \leq y \leq T \end{cases} \quad (22)$$

and its Fourier series expansion is given by (Tolstov, 1962)

$$r_{bin}(x, y) = \frac{a}{(2\pi)^2} \sum_{m, n=-\infty}^{\infty} \frac{[(-1)^n - 1]}{mn} \exp[i\omega_0(mx + ny)], \quad (23)$$

where T and a are the grating period and the amplitude, respectively. Then the intensity profile at the focal plane is calculated from equations (17) and (21), with $r(x, y)$ as vertical binary grating of equation (23), giving (Mora-González et al., 2009)

$$I_{bin}(u, v) = h_0^2 \sum_{k=-\infty}^{\infty} \left(\frac{\sin\left(k\frac{\pi}{2}\right)}{k\frac{\pi}{2}} \right)^2 \cdot \delta\left[Ku, K\left(v - \frac{k\omega_0}{K}\right)\right], \quad (24)$$

here $h_0 = \frac{2Aa\pi^2}{f\lambda}$ is the zero diffraction order amplitude, $K = \frac{2\pi}{f\lambda}$ is the scale factor at the focal plane and $\omega_0 = \frac{2\pi}{T}$ is the angular frequency. The binary grating intensity profile presents an infinite number of diffraction orders (harmonics) modulated by a sinc function (see figure 14b).

3.2.2 Sinusoidal grating

In order to observe the sinusoidal grating profile, it must be above x axis because negative gsl cannot be observed. The equation proposed for the vertical sinusoidal grating is given by (see figure 14c)

$$r_{\sin}(x, y) = a \left[\frac{1}{2} + \frac{1}{2} \sin(\omega_0 y) \right]. \quad (25)$$

The intensity profile at the focal plane from equation (21) with $r(x, y)$ as vertical sinusoidal grating of equation (25), giving (Mora-González et al., 2009)

$$I_{\sin}(u, v) = h_1^2 \delta \left[Ku, K \left(v + \frac{\omega_0}{K} \right) \right] + h_0^2 \delta [Ku, Kv] + h_1^2 \delta \left[Ku, K \left(v - \frac{\omega_0}{K} \right) \right], \quad (26)$$

where $h_1 = \frac{Aa\pi^2}{f\lambda}$ is the ± 1 sinusoidal diffraction orders amplitude. The sinusoidal grating intensity profile only presents three diffraction orders (see figure 14d), those harmonics are characteristic of the Fourier transform of sinusoidal functions.

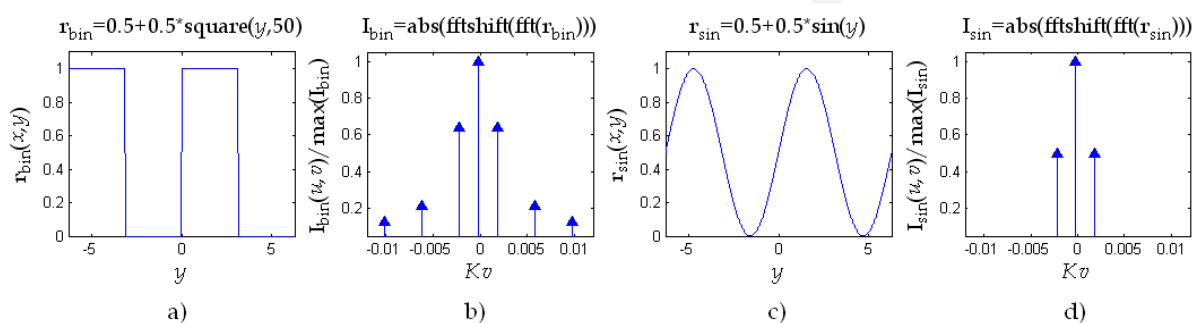


Fig. 14. Functions of a) binary and c) sinusoidal gratings. Fourier spectra of b) binary and d) sinusoidal gratings.

4. Applications

As shown in previous sections, Digital Image Processing is a useful tool to obtain improved results in Optical Metrology. Applications details are presented in following subsections.

4.1 Fringe analysis

Fringe analysis refers to the process of finding the phase associated to physical variables that are being estimated. A typical case consists in the interpretation of the fringe patterns that can be achieved with phase shifting techniques, when the object under study remains static while three or more frames are acquired when the experiment conditions are free of environmental perturbations. Another case is when the environmental conditions are not met, and then the analysis of a single interferogram is more convenient. In both cases a wrapped phase is obtained before the related continuous phase is assessed.

Phase unwrapping is a numerical technique for retrieving a continuous phase from the calculated phase by using the arctangent (atan2) of the sine and cosine functions of the phase. In its simplest form, phase unwrapping consists in the addition or subtraction of a 2π multiple when a discontinuity bigger than π is found between adjacent pixels (Robinson, 1993). This approach however is very sensitive to noise, and is said to be path dependent. It means that any error may propagate along the path followed to phase unwrapping. In this study we will review the least square method (Ghiglia, 1998). Basically, it consists in the integration of the phase gradient by solving a linear equation system employing a numerical technique. Lets assume $\phi^x(x, y)$ and $\phi^y(x, y)$ as the phase differences in the horizontal and vertical directions, respectively. These phases are calculated from the wrapped phase $\phi^w(x, y)$ as follows:

$$\phi^x(x, y) = \tan^{-1} \left\{ \frac{\sin[\phi^w(x, y) - \phi^w(x-1, y)]}{\cos[\phi^w(x, y) - \phi^w(x-1, y)]} \right\} p(x, y) p(x-1, y), \quad (27)$$

and

$$\phi^y(x, y) = \tan^{-1} \left\{ \frac{\sin[\phi^w(x, y) - \phi^w(x, y-1)]}{\cos[\phi^w(x, y) - \phi^w(x, y-1)]} \right\} p(x, y) p(x, y-1), \quad (28)$$

In the above equations $p(x, y)$ is a pupil function equal to one inside of an interferogram field and zero otherwise. A discretized Laplacian equation is then obtained from the phase differences:

$$\begin{aligned} L(x, y) &= \phi^x(x+1, y) - \phi^x(x, y) + \phi^y(x, y+1) - \phi^y(x, y) \\ &= -4\phi(x, y) + \phi(x+1, y) + \phi(x-1, y) + \phi(x, y+1) + \phi(x, y-1) \end{aligned} \quad (29)$$

This equation represents a linear equations system that can be solved with iterative algorithms. In particular, is employed an overrelaxation method (SOR) due to it may be easily programmed. The following equation is then iterated until the solution converges:

$$\begin{aligned} \phi^{k+1}(x, y) &= \phi^k(x, y) + \\ &+ \frac{[d\phi^k(x, y) - \phi(x+1, y) - \phi(x-1, y) - \phi(x, y+1) - \phi(x, y-1) + L(x, y)]r}{d}, \end{aligned} \quad (30)$$

where, $d=p(x+1,y)+p(x-1,y)+p(x,y+1)+p(x,y-1)$, and r is a parameter of the SOR method that must be set between the [1,2] range. Figure 15 shows the wrapped phase ϕ^w obtained from the sine and cosine of the phase and the unwrapped phase ϕ . A simple iterative algorithm that unwraps the phase from the discretized Laplacian is given as:

Algoritm 1. % Unwraps phase.

while (q<max)%q is the number of iterations (500 for this case)

q=q+1;

for i=1:n

for j=1:m

if p(i,j)==1

t=p(i+1,j)+p(i-1,j)+p(i,j+1)+p(i,j-1);

g(i,j)=g(i,j)-((t*g(i,j)-g(i+1,j)-g(i-1,j)-g(i,j+1)-g(i,j-1)+L(i,j))*1.95/t);%iterated equation

else

g(i,j)=0;

end,end,end,end

A single interferogram with open fringes may also be analyzed for phase recovering (Creath & Wyant, 1992). Experimentally an open fringe interferogram can be achieved if a tilt term is added to the phase, usually by tilting the reference beam in an interferometer. Equation (18) can be modified in order to include a tilt term in the x direction, this is as follows:

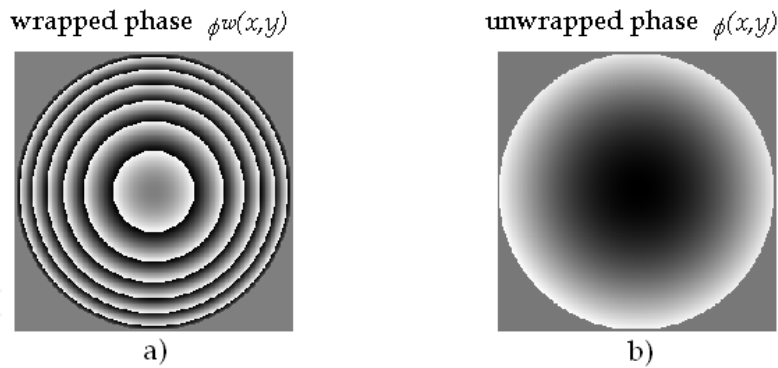


Fig. 15. a) wrapped and b) unwrapped phase.

$$I(x,y) = a(x,y) + b(x,y) \cos[\phi(x,y) + 2\pi tx] \quad (31)$$

where $a(x,y) = I_1(x,y) + I_2(x,y)$ is known as the background intensity and $b(x,y) = 2[I_1(x,y)I_2(x,y)]^{1/2}$ is the modulation or visibility term. The Fourier transform of the expression below can be written as:

$$\tilde{I}(u,v) = \tilde{a}(u,v) + C(u+t,v) + C^*(u-t,v). \quad (32)$$

Then the Fourier spectra of an open fringe interferogram contains three terms, $\tilde{a}(u,v)$ is a narrow peak at the center of the Fourier spectra and $C(u+t,v)$ and $C^*(u-t,v)$ are shifted complex conjugate intensities symmetrically located respect to the origin of the Fourier

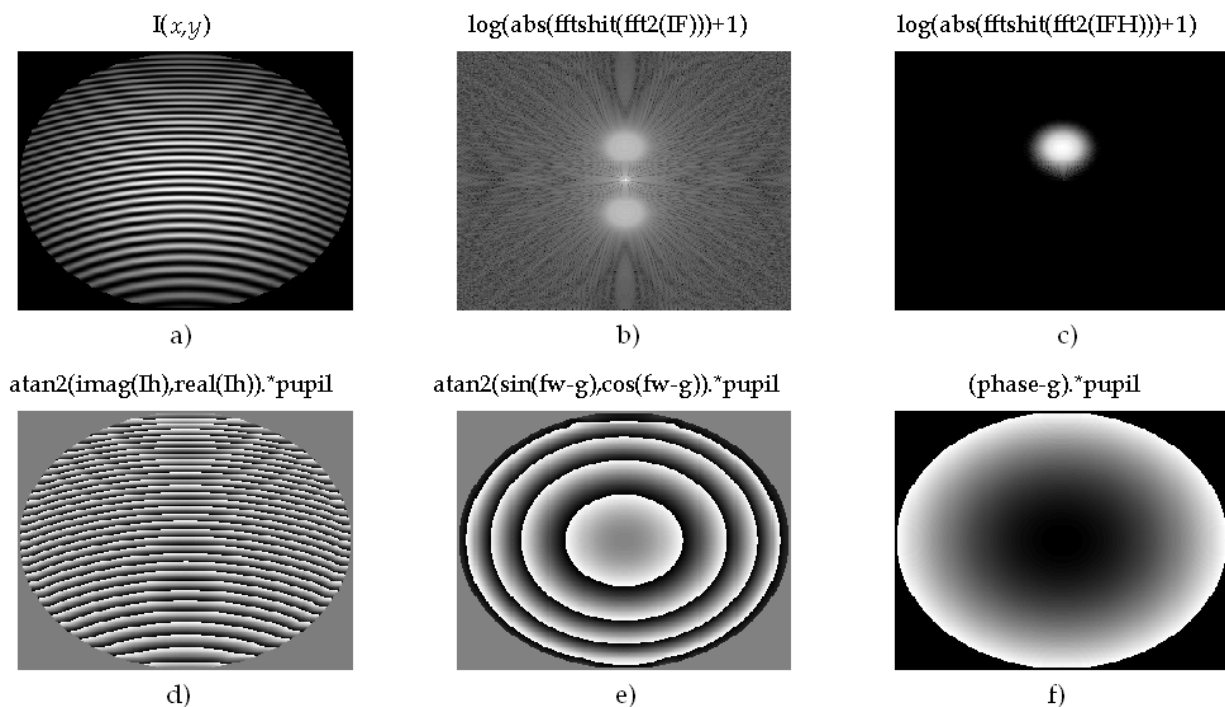


Fig. 16. Process of phase recovery from a single interferogram with closed fringes, as shown in algorithm 2. a) Interferogram, b) Fourier spectrum, c) filtered Fourier spectrum, d) wrapped phase with tilt, e) wrapped phase without tilt, and f) unwrapped continuous phase.

domain (Takeda, 1982). The Fourier procedure to recover the phase consist in isolating either $C(u,v)$ or $C^*(u,v)$. Then the inverse transform is taken in order to retrieve the wrapped phase from the imaginary and real parts of the filtered spectra. The last step, as done with phase shifting procedures, is to apply a phase unwrapping procedure to recover the continuous phase. The complete process of phase recovery from an open fringe interferogram is observed in figure 16.

```

Algorithm 2. % Phase recovery from a single interferogram
for i=1:256
  for j=1:256
    if sqrt((i-128)^2+(j-128)^2)<126 %creates a function pupil
      pupil(i,j)=1;
    else
      pupil(i,j)=0;
    end
    x=(i-128)/128;
    y=(j-128)/128;
    phase(i,j)=2*pi*(4*(x^2+y^2)+16*x);
    g(i,j)=2*pi*16*x;
    back(i,j)=128*exp(-1*(x^2+y^2));
    mod(i,j)=127*exp(-1*(x^2+y^2));
    I(i,j)=(back(i,j)+mod(i,j)*cos(phase(i,j)))*pupil(i,j); % Interferogram with closed fringes
    H(i,j)=exp(-180*((x-0.25)^2+y^2)); % Band-Pass filter
    G(i,j)=1-exp(-1000*(x^2+y^2)); % High pass filter
  end,end
  IF=fftshift(fft2(I)); %Fourier transform of the interferogram
  IFH=IF.*H.*G; %Filtered Fourier transform
  Ih=ifft2(fftshift(IFH)); %Inverse Filtered Fourier transform
  fw=atan2(imag(Ih),real(Ih)).*pupil; %Wrapped phase with tilt
  fw1=atan2(sin(fw-g),cos(fw-g)).*pupil; %Wrapped phase without tilt
  phase1=(phase-g).*pupil; %Unwrapped phase

```

4.2 Wavefront deformation analysis

Optical metrology applied for the determination of different physical variables has greatly contributed with the constant advance of technology at a point that it is becoming a powerful measurement alternative for the solution of problems in engineering and sciences.

4.2.1 Deformation analysis using speckle interferometry

In this section, is presented a deformation analysis for the estimation of out-of-plane displacement components in a simulated model of a cantilever made of aluminum with a load applied at its free end. The example corresponds to a typical problem in structural mechanics where the Young's modulus can be determined from the displacement of the loaded bar made of an isotropic material. The suggested arrangement for the testing in electronic speckle pattern interferometry (ESPI) is shown in figure 17. The laser light beam is divided by the beam splitter BS1. One beam is reflected by a mirror attached to a piezoelectric PZ (PC controlled), and then is expanded to uniformly illuminate at a small

angle respect to the normal of the object surface, and the other beam is coupled into an optical fiber to obtain the reference illumination. The light reflected by the object and the reference beam introduced with BS2 interfere on the CCD.

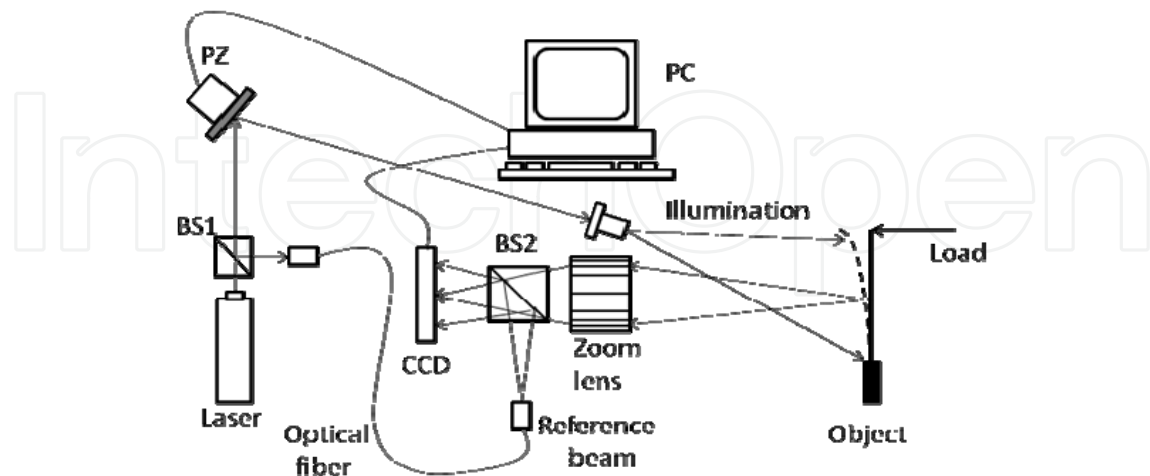


Fig. 17. Electronic speckle pattern interferometer.

The object was simulated by considering the following dimensions: 15 cm length and 3 cm height with a thickness of 0.5 cm. Using the two intensities $I_i(x,y)$, $I_f(x,y)$ of the speckle patterns generated by ESPI arrangement seen in the CCD image plane before and after applying a force of 0.1 N, the correlation fringes using equation (19) is shown in figure 18a and in figure 18b is shown the wrapped phase calculated by equation (20). In figure 18c is shown the filtered and unwrapped phase using a conventional spatial average filter of 3×3 pixels and an iterative least-squares algorithm.

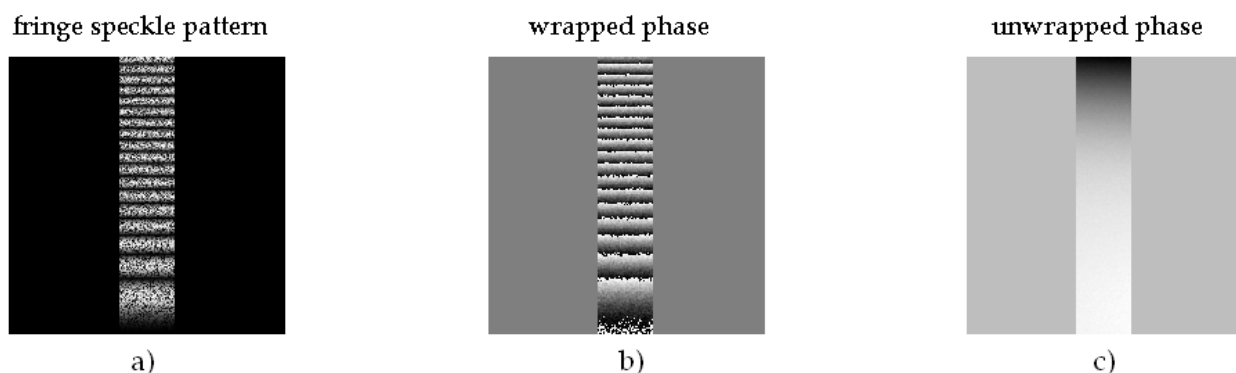


Fig. 18. Deformation analysis of a cantilever with ESPI. a) interference fringe pattern; b) wrapped phase and c) unwrapped phase.

4.3 Wavefront detection

Optical testing using diffraction gratings as wavefront modulators is another alternative to detect wavefront aberrations.

4.3.1 Grating diffraction

Diffraction gratings are optical devices commonly used on physics. There are several gratings types, but as shown in 3.2 section, sinusoidal gratings only diffracts three harmonic

modes, due to this property, sinusoidal gratings have been developed by different techniques. According to the method reported by (Mora-González et al., 2009), is possible to generate these gratings by laser printing on acetates. In figure 19, are shown different increment sizes (Δy) of three sine profiles and the corresponding spectra of equations (25) and (26), respectively. It must be pointed that for larger Δy values, the resolution diminishes and more diffraction orders emerge.

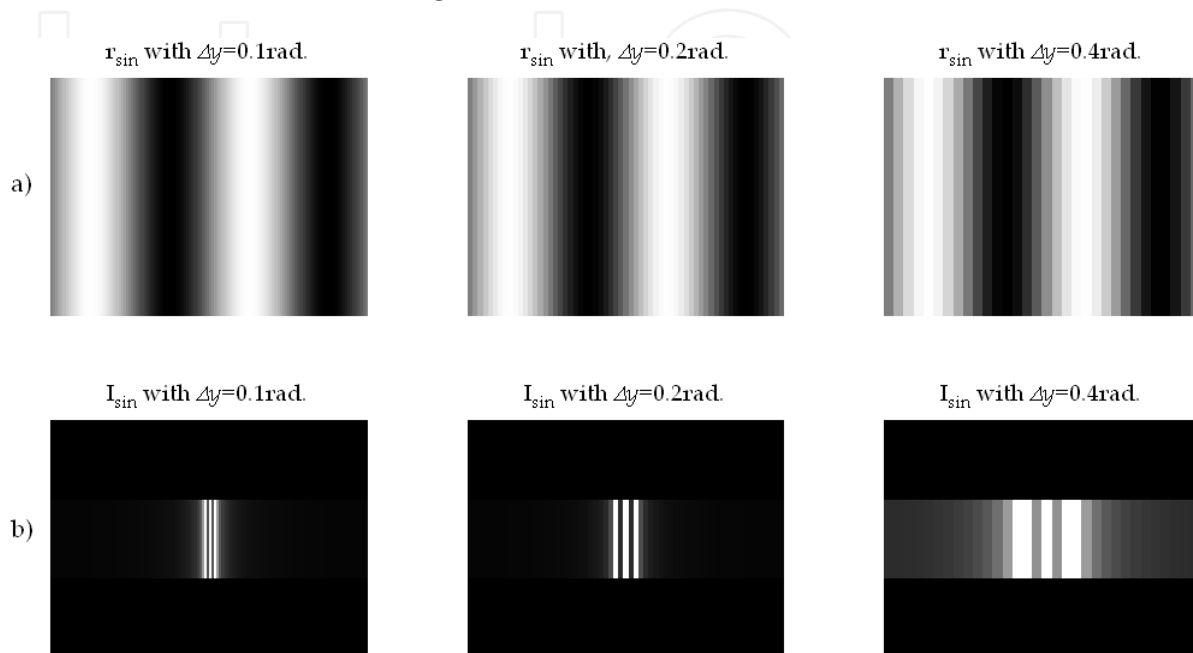


Fig. 19. Sinusoidal gratings generated in Matlab. With a) grating $r_{\sin}=255* [.5+.5*\sin(y)]$ and b) Fourier spectra $I_{\sin}=\text{fftshift}(\text{fft2}(r_{\sin}))$.

4.3.2 Ronchi test

The Ronchi test is one of the most non invasive optical tests used in optical workshops, due to the simplicity for observing aberrations over the optical surface. The test only needs to propagate a convergent aberrated wavefront through a diffraction grating to obtain a modulated fringe pattern (ronchigram) (Mora-González et al., 2001, 2003, 2011). In figure 20 is shown the typical diagram of the Ronchi test using a collimated illumination system. In figure 21 are shown the ronchigram before and after circular low-pass filtering and their corresponding wrapped phase calculated with equation (20).

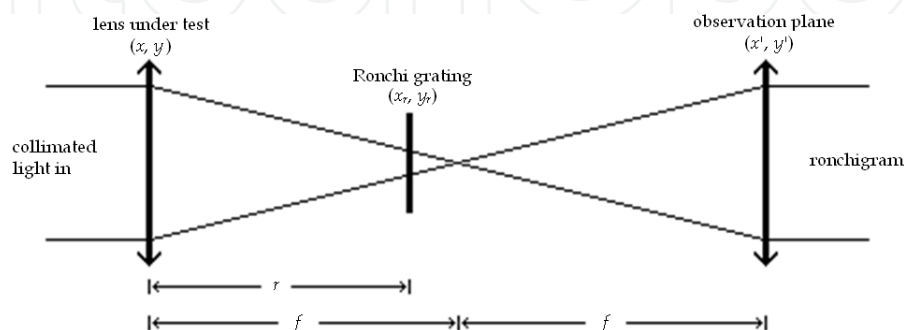


Fig. 20. Collimated light Ronchi test diagram. Where f is the focus of lenses and r is the distance between lens under test and Ronchi grating.

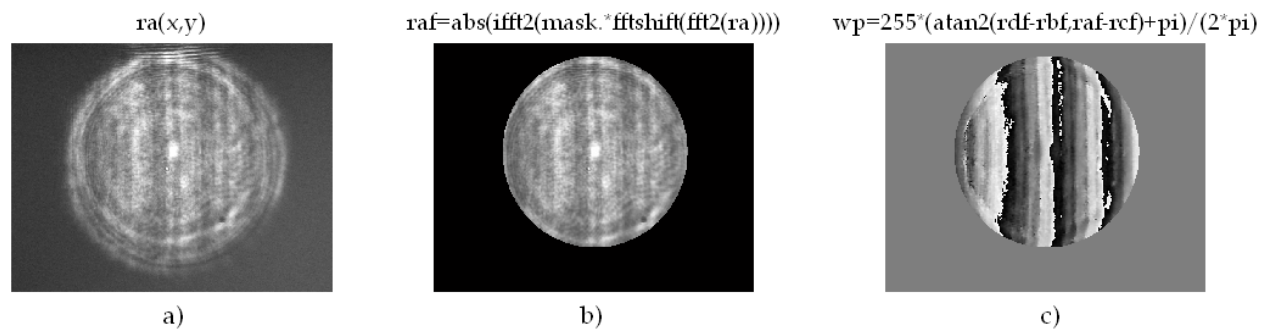


Fig. 21. Ronchi test results. a) ronchigram a: $ra(x,y)$; b) frequency filtered ronchigram a and applied pupil: $raf(x,y)$; and c) wrapped phase of ronchigrams a, b, c and d: $wp(x,y)$.

4.4 Bio-metrology

In the present subsection several functions of Matlab and their applications as blood flow measurement and pattern recognition in fingerprint are shown.

4.4.1 Blood flow measurement

Laser speckle effect is an interference phenomena that is produced when an optical rough surface is illuminated by a laser source that can be observed directly or imaged by using an optical system. The resulting intensity well known as speckle pattern is the result of multiple interferences produced by the roughness of the object under test. The speckle pattern consists in a distribution of brilliant points and dark points.

By assuming ideal conditions like high coherent light source, unique frequency and perfect diffusing surface. It can be proved that the standard deviation of the intensity fluctuations from a speckle pattern is equal to the same that the average of the intensity. Speckle pattern contrast is defined by the relationship between standard deviation (σ) and the averaged intensity (I) (Goodman, 2005):

$$\text{specklecontrast} = \frac{\sigma}{\langle I \rangle}. \quad (33)$$

If the illuminated surface is static, the contrast observed in the speckle pattern is maximum, however, if the surface is moving, the speckle patterns changes completely. This phenomenon is known as “decorrelation” and can be observed when light is dispersed by a great number of moving dispersers, i. e. moving particles into a fluid. The decorrelation is used for fluid velocity quantification considering that a speckle pattern photography taken at a finite time is blurred (contrast losing) in flowing areas. Contrast changes depend on fluid velocity and photography exposure time (T). By assuming a Lorentzian velocity distribution, speckle contrast ($\sigma/\langle I \rangle$) is defined as correlation and exposure time function (τ_c/T).

$$\frac{\sigma}{\langle I \rangle} = \left\{ \frac{\tau_c}{2T} \left[1 - \exp\left(-\frac{2T}{\tau_c}\right) \right] \right\}^{\frac{1}{2}}. \quad (34)$$

Correlation time τ_c is inversely proportional to local velocity of the dispersing particles. The following code calculates a contrast image from a speckle image. Local blood flow velocity

can be found from image contrast information and equation (34). Figure 22 shown speckle images before and after processing.

Algorithm 3. % Calculation of speckle contrast.

```
Im2 = imread('speckle_img.bmp'); % load the bmp image file into the memory.
```

```
Im2 = im2double(Im2);
```

```
windowSize = 5; %define the window size for the filter.
```

```
avgFilter = fspecial('average',windowSize); % generate an averaging filter.
```

```
stdSpeckle = stdfilt(I,ones(windowSize)); %calculates the local standar deviation of image.
```

```
avgSpeckle = imfilter(I,avgFilter,'symmetric'); %calculates the average of each pixel
```

```
ctrSpeckle = stdSpeckle./avgSpeckle; %calculates the speckle contrast image
```

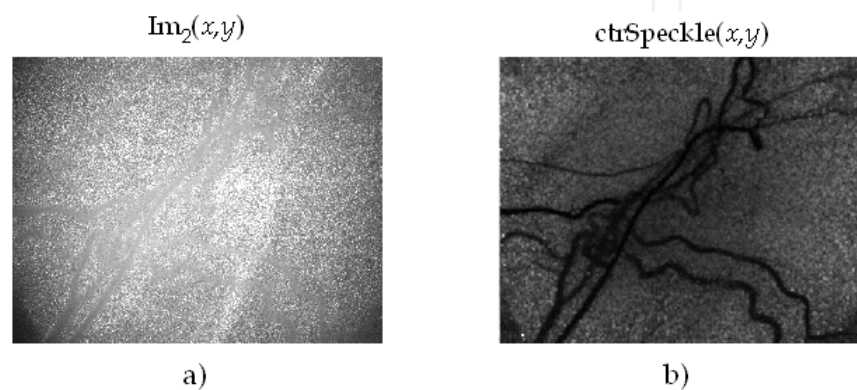


Fig. 22. Blood flow measurement results. a) speckle image of a rat cortex. b) speckle image of contrast after processing with the code of algoritm 3.

4.4.2 Fingerprint measurement

Several applications in pattern recognition are also utilized in optical metrology, finger print parameters measurements is an example. The present subsection shows a new form for fingerprint core determination based in the Radon transform of a fingerprint image, applied in x and y axes directions. The core is located by the interception of the extremes (local minimum and maximum) of the Radon transforms (Mora-González et al., 2010).

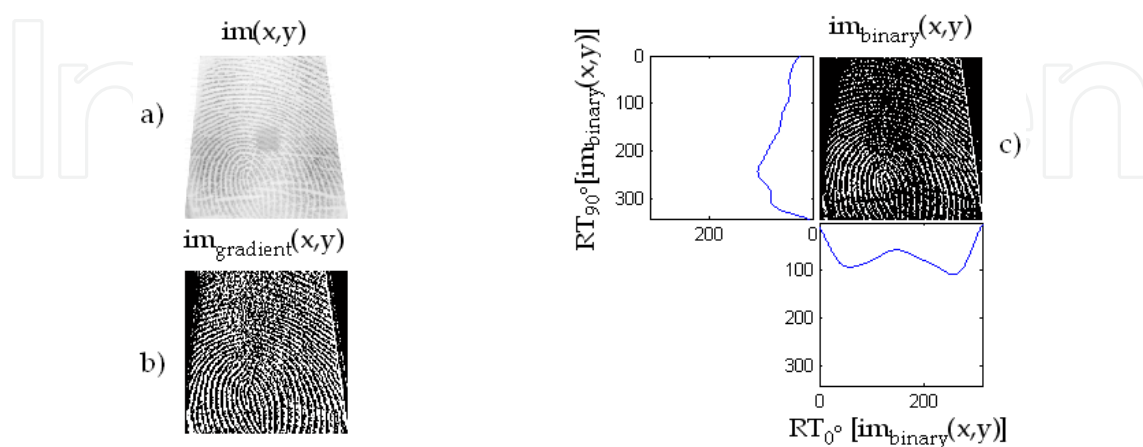


Fig. 23. Images for fingerprint core point detection. a) original fingerprint $im(x,y)$, b) gradient of original fingerprint $im_gradient(x,y)$, and c) binarized gradient $im_binary(x,y)$ and its $0^\circ - 90^\circ$ Radon transforms.

The process for core finding is very simple. First, a high-pass filter with a gradient type convolution mask is applied to a fingerprint image in order to enhance the contrast. Next the image is skeletonized, and the Radon Transform (RT) is applied in the x and y directions to obtain RT_{90} and RT_0 profiles, respectively. Finally, the noise produced from ridges and rows in the fingerprint is minimized by a least-squares algorithm. The whole process is illustrated in figure 23 by using the following algorithm:

```

Algorithm 4. % Fingerprint analysis.
[im,map]=imread(FileName); %read fingerprint
im=double(im); %change image format
[Nx,Ny]=size(im); %image size
im_gradient=gradient(im); %gradient spatial filter
level = graythresh(im_gradient); %finding the threshold of gradient
for x=1:Nx
    for y=1:Ny
        if (im_gradient(x,y)>15*level) %fingerprint skeletonization
            im_binary(x,y)=1;
        else
            im_binary(x,y)=0;
        end,end,end
end,end,end
[RT,xp] = radon(bg,[0 90]); %Radon transform
leastq_0=polyfit(xp,RT(:,1),21); %21° polynomial adjustment for 0° Radon transform
leastq_90=polyfit(xp,RT(:,2),21); %21° polynomial adjustment for 90° Radon transform
y_leastq0=polyval(leastq_0,xp); %least square approximation of 0° Radon transform
y_leastq90=polyval(leastq_90,xp); %least square approximation of 90° Radon transform

```

5. Conclusion

Mathematical fundamentals for Digital Image Processing and their implementation by means of algorithms and Matlab commands were established. It has been demonstrated according to some Optical Metrology applications, the Matlab algorithms efficiency. This confirms that Matlab is a computational powerful tool. However, optical metrology applications are not only limited to the discussed examples in the present chapter. Applications of all the proposed algorithms can be extended without any problem from deformation analysis by another interferometric techniques (Speckle photography, Moiré, etc.) or optical tests (Hartmann, Foucault, etc.), until analysis and pattern recognition in medicine (X-Ray images, tomography, etc.), among other branches of science and engineering.

6. Acknowledgment

The authors wish to express their gratitude for financial support of this project to *Departamento de Ciencias Exactas y Tecnología*, of *Centro Universitario de los Lagos, Universidad de Guadalajara*. The image of figure 22 courtesy of Julio Cesar Ramirez San-Juan, Ph.D (*Instituto Nacional de Astrofísica Óptica y Electrónica*).

7. References

- Bow, S.T. (2002). *Pattern Recognition and Image Preprocessing* (2nd Ed.), Marcel Dekker, Inc., ISBN 0-8247-0659-5, New York, USA.
- Bracewell, R.N. (1995). *Two-Dimensional Imaging*, Prentice Hall, ISBN 0-13-062621-X, New Jersey, USA.
- Canny, J. (1986). A Computational Approach to Edge Detection, *IEEE Trans. on Pattern Analysis and Machine Intelligence*, Vol.PAMI-8, No.6, (November 1986), pp. 679-698, ISSN 0162-8828.
- Creath, K.; Schmit, J. and Wyant, J.C. (2007), Optical Metrology of Diffuse Surfaces, In: *Optical Shop Testing, 3th ed.*, Malacara, D., pp. 756-807, John Wiley & Sons, Inc., ISBN 978-0-471-48404-2, Hoboken, New Jersey, USA.
- Gasvik, K.J. (2002). *Optical Metrology*, John Wiley & Sons, Ltd., ISBN 0-470-84300-4, Chichester, West Sussex, England.
- Ghiglia, D.C., Pritt, M.D. (1998), *Two-Dimensional Phase Unwrapping: Theory Algorithms and Software*, Wiley-Interscience, ISBN 0-471-24935-1, New York, USA.
- Gonzalez, R.C. & Woods, R.E. (2002). *Digital Image Processing* (2nd Ed.), Prentice Hall, ISBN 0-201-18075-8, New Jersey, USA.
- Goodman, J.W. (2005). *Introduction to Fourier Optics* (3rd Ed.), Roberts and Company Publishers, ISBN 0-9747077-2-4, Englewood, USA.
- Huntley, J. M. (2001), Automated analysis of speckle interferograms, In: *Digital Speckle Pattern Interferometry and Related Techniques*, Rastogi, P. K., pp. 59-140, John Wiley & Sons, Ltd., ISBN 0-471-49052-0, Chichester, West Sussex, England.
- Lehmann, M. (2001). Speckle Statistics in the Context of Digital Speckle Interferometry, In: *Digital Speckle Pattern Interferometry and Related Techniques*, Rastogi, P. K., pp. 1-58, John Wiley & Sons, Ltd., ISBN 0-471-49052-0, Chichester, West Sussex, England.
- Mora González, M. & Alcalá Ochoa, N. (2001). The Ronchi test with an LCD grating, *Opt. Comm.*, Vol.191, No.4-6, (May 2001), pp. 203-207, ISSN 0030-4018.
- Mora-González, M. & Alcalá Ochoa, N. (2003). Sinusoidal liquid crystal display grating in the Ronchi test, *Opt. Eng.*, Vol.42, No.6, (June 2003), pp. 1725-1729, ISSN 0091-3286.
- Mora-González, M.; Casillas-Rodríguez, F.J.; Muñoz-Maciel, J.; Martínez-Romo, J.C.; Luna-Rosas, F.J.; de Luna-Ortega, C.A.; Gómez-Rosas, G. & Peña-Lecona, F.G. (2008). Reducción de ruido digital en señales ECG utilizando filtraje por convolución, *Investigación y Ciencia*, Vol.16, No.040, (September 2008), pp. 26-32, ISSN 1665-4412.
- Mora-González, M.; Pérez Ladrón de Guevara, H.; Muñoz-Maciel, J.; Chiu-Zarate, R.; Casillas, F.J.; Gómez-Rosas, G.; Peña-Lecona, F.G. & Vázquez-Flores, Z.M. (2009). Discretization of quasi-sinusoidal diffraction gratings printed on acetates, *Proceedings of SPIE 7th Symposium Optics in Industry*, Vol.7499, 74990C, ISBN 978-0-8194-8067-5, Guadalajara, México, September 2009.
- Mora-González, M.; Martínez-Romo, J.C.; Muñoz-Maciel, J.; Sánchez-Díaz, G.; Salinas-Luna, J.; Piza-Dávila, H.I.; Luna-Rosas, F.J. & de Luna-Ortega, C.A. (2010). Radon Transform Algorithm for Fingerprint Core Point Detection. *Lecture Notes in Computer Science*, Vol.6256, No.1, (September 2010), pp. 134-143, ISSN 0302-9743.
- Mora-González, M.; Casillas, F.J.; Muñoz-Maciel, J.; Chiu-Zarate, R. & Peña-Lecona, F.G. (2011). The Ronchi test using a liquid crystal display as a phase grating, *Proceedings of SPIE Optical Measurement Systems for Industrial Inspection VII*, Vol.8082 part two, 80823G, ISBN 978-0-8194-8678-3, Munich, Germany, May 2011.

- Oppenheim, A.V.; Willsky, A.S. & Nawab, S.H. (1997). *Signals and Systems, 2nd ed.*, Prentice Hall, Inc., ISBN 0-13-814757-4, New Jersey, USA.
- Pratt, W.K. (2001). *Digital Image Processing (3th Ed.)*, John Wiley & Sons, Inc., ISBN 0-471-22132-5, New York, USA.
- Robinson, D.W. (1993). Phase unwrapping methods, In: *Interferogram Analysis*, Robinson, D.W. and Reid, G.T., pp. 195-229, IOP Publishing, ISBN 0-750-30197-X, Bristol, England.
- Sirohi R. S. (1993), *Speckle Metrology*, Marcel Dekker, Inc., ISBN 0-8247-8932-6, New York, USA.
- Takeda, M.; Ina, H. & Kobayashi, S. (1982). Fourier-transform method of fringe-pattern analysis for computer-based topography and interferometry, *J. Opt. Soc. Am.*, Vol.72, No.1, (January 1982), pp. 156-160, ISSN 0030-3941.
- Tolstov, G.P. (1962). *Fourier Series*, Dover Publications, Inc., ISBN 0-486-63317-9, New York, USA.
- Waldner, S. P. (2000). *Quantitative Strain Analysis with Image Shearing Speckle Pattern Interferometry (Shearography)*, Doctoral Thesis, Swiss Federal Institute of Technology, Zurich, Swiss.

IntechOpen



MATLAB - A Ubiquitous Tool for the Practical Engineer

Edited by Prof. Clara Ionescu

ISBN 978-953-307-907-3

Hard cover, 564 pages

Publisher InTech

Published online 13, October, 2011

Published in print edition October, 2011

A well-known statement says that the PID controller is the “bread and butter” of the control engineer. This is indeed true, from a scientific standpoint. However, nowadays, in the era of computer science, when the paper and pencil have been replaced by the keyboard and the display of computers, one may equally say that MATLAB is the “bread” in the above statement. MATLAB has become a de facto tool for the modern system engineer. This book is written for both engineering students, as well as for practicing engineers. The wide range of applications in which MATLAB is the working framework, shows that it is a powerful, comprehensive and easy-to-use environment for performing technical computations. The book includes various excellent applications in which MATLAB is employed: from pure algebraic computations to data acquisition in real-life experiments, from control strategies to image processing algorithms, from graphical user interface design for educational purposes to Simulink embedded systems.

How to reference

In order to correctly reference this scholarly work, feel free to copy and paste the following:

Miguel Mora-González, Jesús Muñoz-Maciel, Francisco J. Casillas, Francisco G. Peña-Lecona, Roger Chiu-Zarate and Héctor Pérez Ladrón de Guevara (2011). Image Processing for Optical Metrology, MATLAB - A Ubiquitous Tool for the Practical Engineer, Prof. Clara Ionescu (Ed.), ISBN: 978-953-307-907-3, InTech, Available from: <http://www.intechopen.com/books/matlab-a-ubiquitous-tool-for-the-practical-engineer/image-processing-for-optical-metrology>

INTECH
open science | open minds

InTech Europe

University Campus STeP Ri
Slavka Krautzeka 83/A
51000 Rijeka, Croatia
Phone: +385 (51) 770 447
Fax: +385 (51) 686 166
www.intechopen.com

InTech China

Unit 405, Office Block, Hotel Equatorial Shanghai
No.65, Yan An Road (West), Shanghai, 200040, China
中国上海市延安西路65号上海国际贵都大饭店办公楼405单元
Phone: +86-21-62489820
Fax: +86-21-62489821

© 2011 The Author(s). Licensee IntechOpen. This is an open access article distributed under the terms of the [Creative Commons Attribution 3.0 License](#), which permits unrestricted use, distribution, and reproduction in any medium, provided the original work is properly cited.

IntechOpen

IntechOpen